Applied Catalysis B: Environmental 98 (2010) 171–179

Contents lists available at ScienceDirect

Applied Catalysis B: Environmental

journal homepage: www.elsevier.com/locate/apcatb

Degradation kinetics of hydroxy and hydroxynitro derivatives of benzoic acid by fenton-like and photo-fenton techniques: A comparative study

Daniela Nichela[a], Ménana Haddou[b], Florence Benoit-Marquié[b], Marie-Thérèse Maurette[b], Esther Oliveros[b], Fernando S. García Einschlag[a,*]

[a] Instituto de Investigaciones Fisicoquímicas Teóricas y Aplicadas (INIFTA, UNLP, CCT La Plata-CONICET), Diag. 113 y 64, Sucursal 4, C.C. 16, (B1900ZAA) La Plata, Buenos Aires, Argentina
[b] Laboratoire des IMRCP, UMR CNRS 5623, Université Toulouse III (Paul Sabatier, UPS), 118 rte Narbonne, F-31062 Toulouse Cedex 9, France

ARTICLE INFO

Article history:
Received 16 January 2010
Received in revised form 30 April 2010
Accepted 25 May 2010
Available online 31 May 2010

Keywords:
Autocatalysis
Photoenhancement
Fe(III) photoreduction

ABSTRACT

The oxidative degradation of a series of hydroxy and hydroxynitro derivatives of benzoic acid by Fenton-like and photo-Fenton processes was compared under identical conditions (initial concentrations, pH and temperature). In spite of closely related chemical structures, (2-hydroxybenzoic (2H-BA), 2,4-dihydroxybenzoic (24DH-BA), 2-hydroxy-5-nitrobenzoic (2H5N-BA), 4-hydroxy-3-nitrobenzoic (4H3N-BA) and 2-hydroxy-4-nitrobenzoic (2H4N-BA) acids), the degradation timescales were remarkably different. A common feature was, however, that autocatalytic decay profiles were displayed by the substrates and H_2O_2. A simple equation, which may be used as a valuable tool for a semiquantitative analysis of the main kinetic features of the inverted "S" profiles, is presented. In addition, a method for the estimation of the relative contribution of photoinduced pathways in photo-Fenton systems (photoenhancement factors) is proposed.

In order to assess the key processes governing the kinetic profiles observed, complementary studies were performed to evaluate the formation of ferric complexes, the reactivity towards $HO^\bullet$ and Fe(II) production efficiencies. Except for 4H3N-BA, the model substrates form highly stable complexes with Fe(III). Competition experiments showed that the reactivities of both the substrates and the ferric complexes with hydroxyl radicals cannot explain the large timescale differences observed in Fenton-like and photo-Fenton systems. The comparison of Fe(II) production under irradiation in the absence of H_2O_2 with the decay profiles observed in both Fenton-like and photo-Fenton systems confirms that the main factor controlling the autocatalytic behavior is the formation of organic intermediates that are capable of reducing Fe(III) species. An additional factor in the photo-Fenton process may be the efficiency of photoinduced Fe(II) production, which is affected by complex formation since the studied complexes exhibit a lower efficiency of Fe(III) photoreduction than the Fe(III)–aquo complex.

1. Introduction

Wastewater treatment by means of advanced oxidation techniques (AOTs) has become one of the issues of major interest in modern environmental chemistry. These techniques are based on the production of reactive species such as hydroxyl radicals ($HO^\bullet$), which are able to oxidize most organic compounds due to their high reactivity and low selectivity [1,2].

In Fenton systems, the production of $HO^\bullet$ radicals mainly occurs through the oxidation of Fe(II) by H_2O_2 (R1). Although the reaction manifold involved in the mineralization process can be quite complex and other species (such as FeO^{2+} and $HO_2^\bullet$) may contribute to the oxidation process, it is widely accepted that the oxidation of organic substrates (S) in Fenton-like systems is coupled with the generation of $HO^\bullet$ radicals through the catalytic decomposition of H_2O_2 in acidic medium. The most important reaction steps include [3–6]:

$$Fe(II) + H_2O_2 \rightarrow Fe(III) + HO^\bullet + HO^- \quad (R1)$$

$$Fe(III) + H_2O_2 \rightleftharpoons [Fe(III)(OOH)]^{2+} + H^+ \rightarrow Fe(II) + HO_2^\bullet + H^+ \quad (R2)$$

$$HO^\bullet + S \rightarrow Products \quad (R3)$$

$$HO^\bullet + H_2O_2 \rightarrow HO_2^\bullet + H_2O \quad (R4)$$

* Corresponding author. Tel.: +54 221 425 7291/7430; fax: +54 221 425 4642.
E-mail address: fgarciae@quimica.unlp.edu.ar (F.S. García Einschlag).

0926-3373/$ – see front matter © 2010 Elsevier B.V. All rights reserved.
doi:10.1016/j.apcatb.2010.05.026

The use of high ferrous salt concentrations may yield almost stoichiometric amounts of HO• radicals (R1). However, this is not advisable because elimination of iron from the aqueous solution at the end of the treatment by a pH increase may generate large amounts of sludge due to precipitation of amorphous ferric oxyhydroxides [7]. The study of Fenton systems with catalytic iron concentrations is of special interest since the use of rather low concentrations of iron salts (e.g., 100 times smaller than $[H_2O_2]$) may be feasible and results in a remarkable reduction of sludge volumes. Under these conditions, the overall reaction rate is generally governed by the Fe(III) reduction stage of the catalytic cycle, as the apparent rate constant of the overall Reaction (R2) (k_2) is much smaller than k_1 [8,9]. Since both Fe(II) and Fe(III) species are simultaneously involved in the catalytic cycle, Fe(III) may also be used to initiate the reaction (Fenton-like process). It is important to mention that if low Fe(III) concentrations are used for the H_2O_2-mediated degradation of aromatic compounds, kinetic profiles displaying autocatalysis are frequently observed [8,10–18]. Interestingly, although the key reactions involved have been firmly established, very often the autocatalytic behavior has not been discussed from a kinetic point of view or has been overlooked.

The strategy most frequently used in Fenton systems to remarkably increase the overall reaction rates and substantially improve the mineralization efficiencies is the use of UV and/or visible irradiation (i.e., photo-Fenton process) [19–21]. The enhancement is mostly due to the photolysis of Fe(III) complexes, such as aquocomplexes and complexes with organic ligands, which dissociate in the excited state to yield Fe(II) and an oxidized ligand [22].

In the present work, Fenton-like and photo-Fenton techniques have been applied to the degradation of a set of hydroxy and hydroxynitro derivatives of benzoic acid. The group of structurally related substrates (S) includes 2-hydroxybenzoic (2H-BA), 2,4-dihydroxybenzoic (24DH-BA), 2-hydroxy-5-nitrobenzoic (2H5N-BA), 4-hydroxy-3-nitrobenzoic (4H3N-BA) and 2-hydroxy-4-nitrobenzoic (2H4N-BA) acids. The substrates were chosen for their structural features, which allow a comparative analysis of the effects of both the nature and the position of the substituents. In addition, the selected compounds are of interest from an environmental viewpoint. Benzoic acid derivatives bearing *ortho*-hydroxyl groups are pollutants [23] ubiquitous in many industrial waste streams [18,24] and nitroaromatic compounds are highly relevant because of their toxicity and relatively low biodegradability [25].

The aim of this study was to compare the kinetic behavior of the autocatalytic profiles observed for the evolution of the concentrations of model substrates, H_2O_2 and total organic carbon (TOC) for this family of structurally related compounds, in both Fenton-like and photo-Fenton systems using identical reaction conditions (initial values of temperature, pH, [Fe(III)], $[H_2O_2]$ and [S]). We have investigated different factors that may influence the kinetic evolution of the model substrates: their acid–base properties, the formation of ferric complexes, the effects of complexation on both the reactivity towards HO• radicals and Fe(III) photoinduced reduction, and the ability of each substrate to yield Fe(III)-reducing species as intermediate degradation products. In addition, we propose simple mathematical tools that may be useful for both a semiquantitative analysis of the complex kinetic profiles obtained and the evaluation of the contribution of photoinduced pathways.

2. Materials and methods

2.1. Reagents

2-Hydroxybenzoic acid >98% (salicylic acid, 2H-BA) and 2,4-dihydroxybenzoic acid ≥98% (24DH-BA) from Fluka, 2-hydroxy-5-nitrobenzoic acid 99% (2H5N-BA), 4-hydroxy-3-nitrobenzoic acid 98% (4H3N-BA) and 2-hydroxy-4-nitrobenzoic acid 97% (2H4N-BA) from Aldrich were used without further purification. H_2O_2 (perhydrol 30%, Merck), H_2SO_4 (98%, Merck), $HClO_4$ (71%, Merck), NaOH (99%, Merck), $FeCl_3$ (anhydrous 99%, Sigma), $Fe(ClO_4)_2 \cdot H_2O$ (98%, Aldrich) and $Fe(ClO_4)_3 \cdot H_2O$ (chloride <0.01%, Aldrich) were used as received. HPLC–grade acetonitrile (ACN) was purchased from Merck. Analytic air was supplied by AGA. Solutions were prepared using Milli-Q purified water (Millipore). Great care was taken to prepare Fe(III) stock solutions that were immediately used in order to prevent Fe(III) precipitation. The pH of the solutions used in kinetic and complexation experiments was adjusted to a value of 3.0 with $HClO_4$ (0.5 M), whereas for the acid–base equilibrium studies both $HClO_4$ (0.1 M) and NaOH (0.1 M) were used.

2.2. Analytical methods

Absorption spectra were recorded using a Cary 3 double-beam spectrophotometer from Varian or an HP-8452A diode-array single beam spectrophotometer from Hewlett Packard. The pH of the solutions was monitored using a Radiometer pH meter (model PHM220). Quantification of the substrates in the reaction mixtures was performed by HPLC using a Shimadzu instrument (solvent delivery module LC-20AT, online degasser DGU-20A5, UV–vis photodiode array detector SPD-M20A, column oven CTO-10 A5 VP, autosampler SIL-20AAT) equipped with an Alltech Prevail Organic Acid 5 μ column (RP-C18, 150 mm long × 4.6 mm i.d.). The column temperature was maintained at 25 °C. The mobile phases were prepared by mixing different proportions of ACN with an aqueous buffer at pH 3 (11 mM H_3PO_4 and 6.4 mM triethylamine). Two mobile phases, composed of 10/90 and 25/75 (v/v) ACN/aqueous buffer, were used. The flow rate was 1 mL min^{-1}. The evolution of the total organic carbon (TOC) was monitored using a Shimadzu instrument (5000A TOC analyzer, catalytic oxidation on Pt at 680 °C). The concentration of H_2O_2 was measured using a colorimetric test [26]. Fe(II) concentrations were quantified by a colorimetric technique through the complex formed with o-phenanthroline [27].

2.3. Experimental procedures and setup

Experimental results presented in this work showed good reproducibility and correspond to runs repeated at least 2 or 3 times under the same conditions.

2.3.1. Spectrophotometric characterization of acid–base and complexation equilibria

Preliminary tests were performed in order to characterize the acid/base properties of the model substrates, the formation of complexes with Fe(III) and the acid/base properties of these complexes. The absorption spectra of 0.65 mM solutions of each substrate in the absence of Fe(III) were recorded from pH 1.5 to pH 5.5. The values of the first deprotonation constants (pK_{a1}) were estimated by nonlinear fitting of the absorbance versus pH profiles obtained at selected wavelengths (Section A, Supporting Data). The formation of Fe(III)-complexes in aqueous solutions was studied at pH 3 (near optimal condition for the Fenton processes [6,21]), using substrate and Fe(III) concentrations ranging from 0 to 3.0 mM and 0 to 3.5 mM, respectively. Conditional formation constants (i.e., pH 3.0) for the 1:1 complexes were estimated by nonlinear fitting of the absorbance versus [Fe(III)] profiles obtained at the maximum wavelengths corresponding to each ferric complex (Section B, Supporting Data). Finally the acid/base properties of the ferric complexes were studied between pH 2.0 and 4.0 using concentrations ranging from 0.1 to 0.2 mM. Characterization tests were carried out at room temperature and without control of the ionic strength.

2.3.2. Evaluation of reactivity towards HO•

Competition experiments were planned to assess the reactivity of both the substrates and their Fe(III) complexes towards HO• radicals. Competition kinetics are routinely used to compare the reactivities of solutes present together in the same solution and, thus, under strictly identical conditions [28]. Accordingly, the analysis of the decay profiles of different compounds within the same environment is a means to evaluate their relative reactivity [29]. In the present work, competition experiments were performed at pH 3.0 using two different methods for HO• radical production (UV/H_2O_2 and $Fe(III)/H_2O_2$) in order to compare relative reactivities in the absence and in the presence of Fe(III). Since the substrate 4H3N-BA does not form stable complexes with Fe(III) under the conditions tested, it was considered as the reference compound for the entire set of competition tests. Based on the chemical nature of the different substrates, two mixtures were used to compare reactivities for both iron-free and ferric solutions. Mixture A (M_A) was prepared with 2H-BA, 2H4N-BA and 4H3N-BA (0.67 mM), whereas Mixture B (M_B) was prepared with 24DH-BA, 2H5N-BA and 4H3N-BA (0.67 mM). The following elution conditions were used to obtain optimal chromatographic resolution for each mixture: 20/80 ACN/aqueous buffer (aqueous buffer: 13 mM TEA, 44 mM H_3PO_4, pH 2).

The UV/H_2O_2 competition tests were performed in a batch reactor similar to that used for photo-Fenton experiments (see below), but using a cooling sleeve made of quartz instead of Pyrex. Two sets of conditions were employed in UV/H_2O_2 tests: (i) $[acid]_0 = 0.67$ mM for all acids and $[H_2O_2]_0 = 145$ mM (very fast reactions were observed in this case); (ii) $[acid]_0 = 0.22$ mM and $[H_2O_2]_0 = 49$ mM. Owing to the large excess of H_2O_2 relative to the concentration of the organic substrates, the incident radiation was almost exclusively absorbed by H_2O_2. The $Fe(III)/H_2O_2$ competition tests were performed using an excess of Fe(III) (2.0–2.3 mM) relative to the concentrations of acids (0.5 mM). Given the relatively high H_2O_2 and iron concentrations used, the reaction was very fast. Therefore hydrogen peroxide was added in two to four successive fractions (40–50 μL of a 11.0 M stock solution) and samples were taken a few minutes after each addition.

Relative rate constants were obtained by plotting $\ln[S_i]$ against $\ln[S_{Ref}]$, as described in a previous paper [29], the substrate 4H3N-BA being the internal reference (Ref.). Further details are given in Section C of the Supporting Data.

2.3.3. Kinetic studies

Dark Fenton-like experiments were carried out at 24 ± 2 °C in a 200 mL batch reactor, covered with an aluminum foil to avoid ambient light effects. Photo-Fenton experiments were performed in a Pyrex batch reactor equipped with two sampling ports and a recirculation circuit for temperature control (25 ± 3 °C). A medium pressure mercury arc lamp (Philips HPK 125) was used as radiation source. The initial pH for all tests was 3.0. During the course of the kinetic runs a small pH decrease until values of *ca.* 2.6 was observed, then the pH increased to a final value of 2.8. The initial concentrations of the substrates, Fe(III) and H_2O_2, were varied from 0.25 to 2.3 mM, from 0.1 to 1.0 mM and from 2.0 to 8.0 mM, respectively. Hydrogen peroxide was added immediately before the start of each experimental run. All experiments were performed under continuous stirring and air bubbling. The degradation profiles were studied by measuring the time evolution of the UV/vis spectra, HPLC peak areas, H_2O_2 concentration and TOC. The tests performed to quantify the photoinduced production of Fe(II) were conducted in the absence of H_2O_2, and the reagents were kept in the dark before starting irradiation in order to avoid Fe(II) formation during sample preparation and reactor filling.

Table 1
Estimated pK_{a1} values[a] and fractions of deprotonated forms at pH 3.0.

Compound	pK_{a1}	pK_{a1} (Literature)	α_1, pH 3.0
2H5N-BA	2.1 ± 0.1	1.96–2.31 [30], 1.95 [31]	0.89
2H4N-BA	1.8 ± 0.1	2.31 [32]	0.94
2H-BA (SA)	2.9 ± 0.1	2.57–3.10 [30], 2.98 [33]	0.56
24DH-BA	2.6 ± 0.2	2.62 [31]	0.72
4H3N-BA	3.6 ± 0.1	–	0.20

[a] Since ionic strength was not adjusted, the pK_a obtained are only estimates of the true thermodynamic values.

3. Results and discussion

3.1. Substrate characterization

3.1.1. Acid–base equilibria

The study of the absorption spectra of the investigated benzoic acid derivatives, for pH values ranging from 1.5 to 5.5, shows an important effect of the substituents on the acid dissociation constant of the carboxyl group (i.e., pK_{a1}). The results (Section A, Supporting Data) indicate that, at pH 3.0 and in the absence of Fe(III), depending on the substrate there are significant differences in the relative fractions of the protonated and deprotonated forms (α_0 and α_1, respectively):

$$LH_2 \rightarrow LH^- + H^+ \quad (R5)$$

where LH_2 was used as a general notation for the model substrates investigated.

The estimated pK_{a1} values (Table 1) are in good agreement with literature values [30–33] and show that, except for the substrate 4H3N-BA, the deprotonated carboxylate forms prevail at pH 3.0.

3.1.2. Fe(III)-complexation studies

The analysis of UV/vis data of Fe(III)-containing solutions of the different substrates (Section B, Supporting Data) shows that, except for 4H3N-BA, highly stable complexes with stoichiometry 1:1 are formed at pH 3.0:

$$LH^- + Fe(III) \rightarrow [Fe(III)L]^+ + H^+ \quad (R6)$$

Fig. 1 presents the normalized absorbance profiles as a function of the ratio [substrate]/[Fe(III)] for the wavelengths corresponding to the absorption maxima of the ligand-to-metal charge transfer (LMCT) bands typical of each complex (i.e., 486 nm for 2H5N-BA and 2H4N-BA, 526 nm for 2H-BA and 514 nm for 24DH-BA). The comparison of the chemical structures of the model substrates indicates that the formation of highly stable Fe(III) complexes requires the presence of the hydroxyl group in *ortho* position with respect to the carboxyl group, both groups participating in the complexation.

It should be noted that the substrates 2H5N-BA and 2H4N-BA may also form complexes with stoichiometry 2:1, as shown by the absorption changes beyond the 1:1 concentration ratio. This behavior was not observed in the absence of a nitro group on the aromatic ring.

Finally, the spectral analysis of the solutions of the ferric complexes from pH 2.0 to 4.0 did not show significant changes. This behavior suggests that, in the pH range relevant to Fenton systems, there is only one important species regarding acid–base equilibrium of the ferric complexes.

3.1.3. Reactivity towards hydroxyl radicals

The reactivity of the substrates and their Fe(III) complexes towards HO• radicals was assessed by means of competition experiments, conducted in the absence and in the presence of Fe(III), and using two different substrate mixtures (M_A and M_B), both containing 4H3N-BA as a reference compound. The relative reactivities

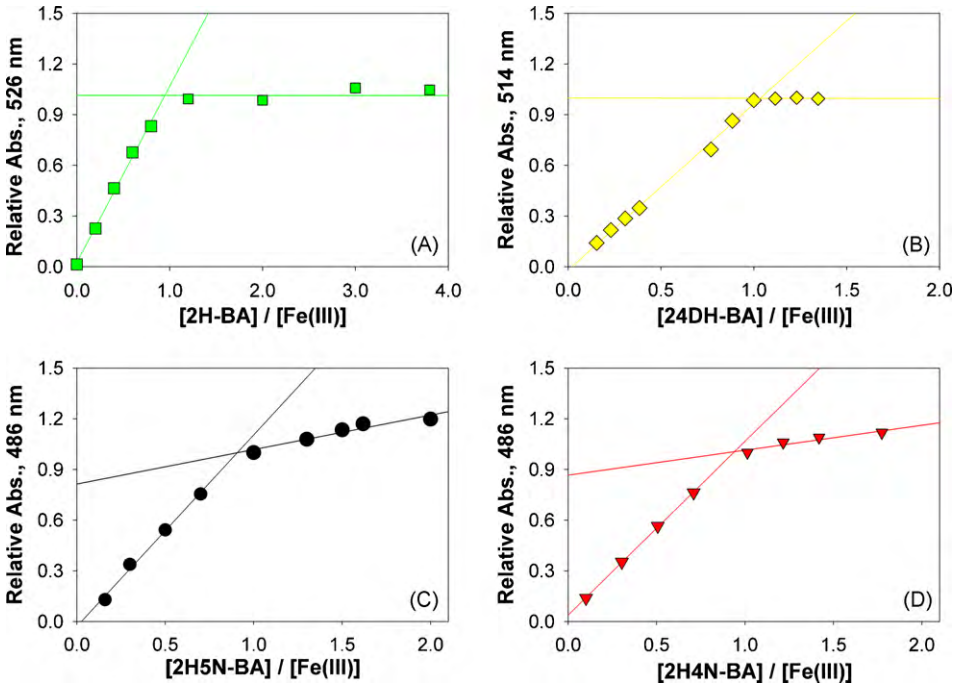

Fig. 1. Normalized absorbance of the LMCT band maximum against the ratio [substrate]/[Fe(III)]. (A) 2H-BA, [Fe(III)] = 0.1 mM. (B) 24DH-BA, [Fe(III)] = 2.6 mM. (C) 2H5N-BA, [Fe(III)] = 1.2 mM. (D) 2H4N-BA, [Fe(III)] = 1.2 mM.

calculated for both UV/H_2O_2 and Fe(III)/H_2O_2 systems are listed in Table 2.

The results clearly show that the reactivities of the Fe(III) complexes do not differ in any case by more than 30% from those corresponding to the free substrates. Thus, complexation of the substrates with Fe(III) cannot exert a dominant effect on their stability in Fenton systems. Interestingly, the interaction with Fe(III) seems to activate the nonnitrated substrates (2H-BA and 24DH-BA), since their Fe(III) complexes are more reactive towards HO• than the free acids. This result is in contrast with the suggestion that HO• radicals mostly attack uncomplexed substrate molecules [18]. On the other hand, the formation of Fe(III) complexes by the nitrated compounds decreases their reactivity. It is worth mentioning that, given the experimental design of the competition tests, each competition mixture (M_A and M_B) contained, besides the reference compound, a nitrated compound together with a nonnitrated one; nevertheless, the reactivity results are grouped into nitrated and nonnitrated substrates.

The results presented in Table 2 show that the reactivity orders of the studied substrates towards HO• at pH 3.0 for their uncomplexed forms (Fe(III)-free systems) and their ferric complexes follow the trends:

2H4N-BA > 2H5N-BA > 2H-BA ≈ 24DH-BA > 4H3N-BA (uncomplexed)
24DH-BA ≈ 2H-BA > 2H4N-BA > 2H5N-BA > 4H3N-BA (1 : 1 complexes)

Although there are observable differences in the measured rate constants, the differences among the most reactive and the least reactive substrates are not larger than 40%, the reactions of all substrates with HO• radicals being almost diffusion-controlled (Table 2).

3.2. Autocatalytic degradation of the substrates in Fenton-like systems

With the aim of characterizing the degradation kinetics of the model substrates (S) in Fenton-like and photo-Fenton systems, the evolution of [S], [H_2O_2] and TOC profiles was studied using the same initial conditions of reactant concentrations, pH and temperature. Concentration profiles in these systems often display a complex autocatalytic-type kinetic behavior with an initial slow phase followed by a faster phase where the rates of both substrate and H_2O_2 consumption increase considerably [4,13]. The effect of the initial reaction conditions on the kinetic behavior of these systems has already been studied in some cases [4,35]. However, as far as we know, comparative studies on the autocatalytic behavior of substrate families have not been reported.

It should be taken into account that, due to the formation of ferric complexes, up to three different species derived from the model substrates may be present in the initial samples: the ferric complexes ([Fe(III)L]$^+$), the protonated substrates (LH_2) and the deprotonated substrates (LH^-). The relative proportions, which depend on the initial pH and the concentrations of both the substrate and the catalyst, can be obtained using the pK_{a1} values of the substrates and the stability constants of the ferric complexes. The results (Table S1, Supporting Data) show that, under our experimental conditions, almost 80% of the substrates 2H4N-BA and 2H5N-BA and about 90% of the substrates 2H-BA and 24DH-BA are in their free forms (both protonated and deprotonated, i.e., LH_2/LH^-), whereas 4H3N-BA remains uncomplexed. Therefore, it can be shown that the apparent reactivity of the substrates towards HO• in Fenton-like and photo-Fenton systems is practically identical to that observed in Fe(III)-free systems.

3.2.1. Dark Fenton-like systems

The normalized profiles of [S] and [H_2O_2] for the different acids during their degradation in Fenton-like systems are depicted in Fig. 2. The kinetic behavior is strongly dependent on the nature of the substrate and, except in the case of 4H3N-BA, the substrates clearly display autocatalytic decays, the profiles being like inverted S-shaped curves. In the analyzed time scales, the substrates are totally exhausted, whereas H_2O_2 is not completely consumed (Fig. 2B). In addition, in all cases, the TOC values did not decrease by more than 15% of the initial values (Figure S13a, Supporting Data). Similar trends regarding both the residual H_2O_2 values and the low TOC decrease have been observed in other

Table 2
Relative reactivites and apparent rate constants at pH 3.0 for the reaction of the model substrates with hydroxyl radicals (data obtained by competition experiments[a]).

Mixture	Compound	UV/H_2O_2 systems	Fenton-like systems	Relative[c] difference	k_{UV/H_2O_2} M^{-1} s^{-1}[b,d]	k_{Fenton} M^{-1} s^{-1}[d]
–	4H3N-BA[a]	1.00 (Int. Ref.)	1.00 (Int. Ref.)	0 by def.	1.8×10^{10}	1.8×10^{10}
M_A	2H-BA	1.25 ± 0.13	1.62 ± 0.01	+25.8%	2.2×10^{10} [34]	2.8×10^{10}
M_B	24DH-BA	1.23 ± 0.08	1.63 ± 0.11	+28.0%	2.2×10^{10}	2.9×10^{10}
M_A	2H4N-BA	1.74 ± 0.02	1.53 ± 0.02	−12.8%	3.1×10^{10}	2.7×10^{10}
M_B	2H5N-BA	1.50 ± 0.02	1.22 ± 0.06	−20.6%	2.6×10^{10}	2.1×10^{10}

[a] Since 4H3N-BA does not form complexes with Fe(III), its rate constant of reaction towards HO• was assumed to be independent of the presence of iron. Thus, absolute rate constants in the presence of Fe(III) for the complexes of the remaining acids were obtained using 4H3N-BA as a reference.
[b] The absolute rate constants in the absence of Fe(III) for UV/H_2O_2 systems were obtained using 2.2×10^{10} M^{-1} s^{-1} for salicylic acid (2H-BA).
[c] Relative differences were calculated using the average values as reference (i.e., $2 \times \{k_{Fenton} - k_{UV/H_2O_2}\}/\{k_{Fenton} + k_{UV/H_2O_2}\}$).
[d] Apparent rate constants in UV/H_2O_2 systems correspond to $k(UV/H_2O_2) = \alpha_0 k(LH_2) + (1 - \alpha_0) k(LH^-)$ (where α_0 is the molar fraction of the protonated form), whereas the rate constants obtained in the presence of iron correspond to the complexed species $[Fe(III)L^{-2}]^+$ since there is only one acid–base form of the complexes at pH 3.0 and 1:1 complexes are formed in excess of Fe(III).

Fenton-like systems [16,36]. The slow H_2O_2 consumption and the low efficiencies of mineralization may be attributed to the production of aliphatic carboxy derivatives (such as oxalic and formic acid). These compounds form Fe(III) complexes highly stable in the dark, blocking the catalytic recycling of Fe(II) through the inhibition of Fe(III) reduction by H_2O_2 (Reaction (R2)) [6,36].

It has been shown that the autocatalytic behavior observed in several Fenton systems is due to the formation of reaction intermediates that are capable of reducing Fe(III) species, thus contributing to Fe(II) recycling "in the catalytic mode of Fenton systems" [8,13]. Examples of such intermediates are *ortho*- or *para*-dihydroxybenzene derivatives and their corresponding semiquinone-like radicals as Fe(III) reducing agents [4,13–15,35,37]:

$$Fe(III) + (HO)_2Ar \rightarrow Fe(II) + HOArO^\bullet + H^+ \quad (R7a)$$

$$Fe(III) + HOArO^\bullet \rightarrow Fe(II) + O_2Ar + H^+ \quad (R7b)$$

Therefore, during the initial stages, the reaction rates are controlled by the slow reduction of Fe(III) through Reaction (R2). As the oxidation proceeds, the accumulation of reducing intermediates results in much faster Fe(II) production through reactions such as (R7), and the degradation process enters into the fast phase.

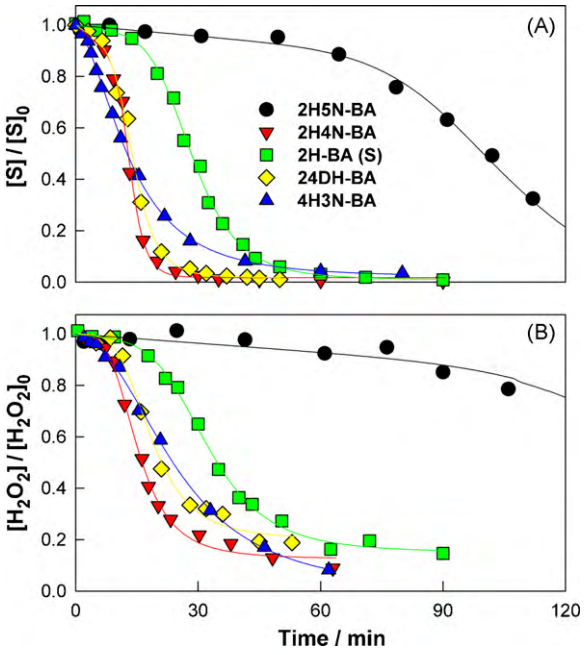

Fig. 2. Normalized concentration profiles obtained in the dark Fenton-like process. (A) Model substrates. (B) H_2O_2. Reaction conditions: $[S]_0 = 1.0$ mM, $[H_2O_2]_0 = 5.2$ mM, $[Fe(III)]_0 = 0.1$ mM, pH 3.0, $T = 25 \pm 2$ °C; the lines were drawn by fitting with Eq. (8).

The quantitative description of kinetic traces with inverted "S" shapes is rather complicated and, to the best of our knowledge, no simple equation has been proposed to model concentration profiles of this kind that are frequently found in degradation studies of environmental relevance. As a tool to examine the observed kinetic curves we used an empirical equation, that is a modification of the "logistic curve" from OriginLab 7.5 (OriginLab Corporation, Northhampton, MA 01060, USA), for fitting the normalized decay profiles:

$$f = \frac{1 - a \times t - d}{1 + (t/b)^c} + d \quad (8)$$

In this equation, the parameters *a*, *b*, *c* and *d* may be employed to characterize the average oxidation rate during the slow phase (hereafter the "normalized initial rate"), the time required to reach half of the initial concentration (hereafter the "apparent half-life"), the average slope during the fast phase and the final residual value, respectively. The solid lines in Fig. 2 show that the equation allows a precise estimation of the temporal dependence of both substrate and H_2O_2 concentration profiles. It should be noted that, despite lacking a precise kinetic meaning, Eq. (8) has a key advantage from a practical point of view: it requires only a few experimental points to draw S-shaped curves that closely describe the complex autocatalytic profiles frequently observed in Fenton-like systems. The fitting of Fig. 2A profiles with Eq. (8) (Table S2, Supporting Data) shows that in dark Fenton-like systems the "normalized initial rates" (a) vary from 1.4×10^{-3} min^{-1} (2H5N-BA) to 1.6×10^{-2} min^{-1} (4H3N-BA). In addition, the "apparent half-lives" (b) vary from 13.6 min (2H4N-BA) to 104 min (2H5N-BA). Similar trends are observed for the H_2O_2 profiles (Fig. 2B).

Although the chemical structures of the substrates are closely related, the degradation timescales are remarkably different. The comparative analysis of the consumption profiles obtained for the different substrates indicates that, during early reaction stages, the depletion rates of the substrates in Fenton-like systems show the following trend:

$$4H3N\text{-}BA > 2H4N\text{-}BA \approx 24DH\text{-}BA > 2H\text{-}BA \gg 2H5N\text{-}BA$$

Surprisingly, under the conditions employed, 4H3N-BA displays the highest initial oxidation rate. This behavior is not correlated with its reactivity towards HO• radicals since competition tests (Section 3.1) showed that the rate constant of its reaction with HO• is the lowest among the series of substrates investigated. Moreover, the latter sequence does not match the trends shown in Table 2 for the reactivities towards HO• radicals. Therefore, the important kinetic differences observed among the substrates cannot be correlated with their differences of reactivity towards HO• radicals either in the presence or in the absence of Fe(III). Other parameters, which play a key role

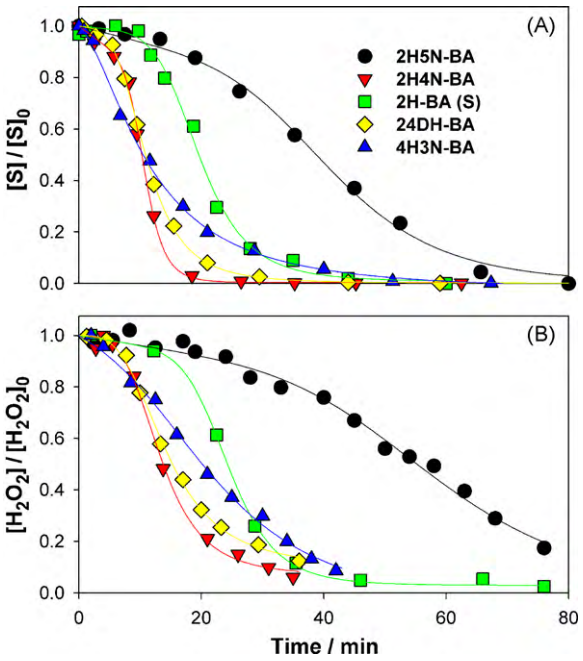

Fig. 3. Normalized concentration profiles obtained in the photo-Fenton process. (A) Model substrates. (B) H_2O_2. Reaction conditions: $[S]_0 = 1.0$ mM, $[H_2O_2]_0 = 5.2$ mM, $[Fe(III)]_0 = 0.1$ mM, pH 3.0, $T = 25 \pm 2$ °C, HPK125 lamp with Pyrex sleeve; the lines were drawn by fitting with Eq. (8).

in the autocatalytic profiles observed, are discussed in Section 3.4.

3.2.2. Photo-Fenton systems

Fig. 3 shows that the decay profiles obtained for [S] and $[H_2O_2]$ in photo-Fenton experiments also display autocatalytic features.

The comparison with the results of Fig. 2 indicates that under irradiation the slow initial phase is shortened. This behavior may be explained taking into account the contribution of photoinduced processes, such as the photoreduction of Fe(III) in the predominant Fe(III)–aquo complex at pH 3 by inner-sphere ligand-to-metal charge transfer (LMCT) [38–40]. At early stages, this process provides an alternative Fe(II) reduction pathway that is faster than Reaction (R2), thus substantially increasing Fe(II) and HO• production rates [37]:

$$[Fe(III)(OH)]^{2+} + h\nu \rightarrow Fe(II) + HO^{\bullet} \quad (R9)$$

The analysis of H_2O_2 profiles during irradiation shows that, in contrast to dark Fenton-like systems, the additive is completely exhausted shortly after the substrate has been totally consumed. In addition, the TOC profiles also exhibit inverted-S shapes (Figure S12, Supporting Data) and, except for the substrate 2H4N-BA, it is generally observed that the times required for 85% TOC diminution are approximately twice the time required for the total consumption of H_2O_2. The aforementioned differences suggest an important contribution of photochemical reactions involving degradation products, such as oxalate and formate anions, which are generated in the final oxidation stages and are capable of forming photoactive Fe(III) complexes [20,36,41]:

$$[Fe(III)(RCOO)]^{2+} + h\nu \rightarrow Fe(II) + CO_2 + R^{\bullet} \quad (R10)$$

The comparison between the different substrates reveals the same reactivity order as observed for Fenton-like systems. The fitting of the normalized HPLC profiles (Fig. 3A) to Eq. (8) shows that, in photo-Fenton systems, the "apparent initial rates" (a) vary from 2.3×10^{-3} min^{-1} (2H-BA) to 1.8×10^{-2} min^{-1} (2H4N-BA), whereas the "apparent half-lives" (b) vary from 11.0 min (2H4N-BA) to 44.4 min (2H5N-BA) (Table S3, Supporting Data). As in the case of dark experiments, similar trends are observed for the H_2O_2 profiles (Fig. 3B).

Table 3
Photoenhancement factors for substrate and H_2O_2 consumption calculated with Eq. (12).

	PEF'_S	$PEF'_{H_2O_2}$
4H3N-BA	29%	16%
2H4N-BA	18%	13%
24DH-BA	20%	24%
2H-BA (S)	30%	25%
2H5N-BA	62%	64%

3.2.3. Photoenhancement factor

With the purpose of making a rough estimation of the relative contribution of photostimulated pathways in photo-Fenton systems, we propose the parameter "photoenhancement factor" (*PEF*) defined by means of the following equation:

$$PEF = \frac{k_{App}^{Phot} - k_{App}^{Dark}}{k_{App}^{Phot}} \quad (11)$$

where k_{App}^{Dark} and k_{App}^{Phot} are the characteristic rate constants associated with the dark and photoenhanced reactions, respectively. The *PEF* is a useful index that allows evaluating the contribution of photoinduced processes in photo-Fenton systems. For simple kinetic profiles, the apparent rate constants would be used to evaluate the *PEF*; nevertheless, the autocatalytic profiles observed in the present work are rather complex and cannot be characterized by means of a single rate constant. Moreover, since *PEF* might be conversion-degree dependent, a global parameter would be a better choice. Therefore, we used the "apparent half-lives" – which can be obtained either from the concentration-time plots (graphical method) or by using Eq. (8) (analytical method) – to define an "overall photoenhancement factor" (PEF_O) by the following relation:

$$PEF_O = 1 - \frac{t_{1/2}^{Phot}}{t_{1/2}^{Dark}} \quad (12)$$

It is worth mentioning that for simple rate laws, regardless of the reaction order, the half-life is always inversely proportional to the rate constant. Thus, the PEF_O values corresponding to the normalized profiles of both substrate and H_2O_2 were calculated by using Eq. (12) for the studied compounds. The values, expressed as percentages, are presented in Table 3.

Except in the case of 4H3N-BA, which clearly exhibits a behavior different from that of the other compounds, the percentage of photochemical enhancement increases with the stability of the substrates in the dark reaction (Fenton-like system):

$$2H5N\text{-}BA \gg 2H\text{-}BA > 24DH\text{-}BA \approx 2H4N\text{-}BA$$

A similar trend (higher photoenhancement for conditions where the dark reaction is slower) has been reported in a previous study on the degradation of nitrobenzene in a range of experimental conditions [37]. This behavior could be interpreted assuming that the rates of the photoinduced reactions mostly depend on the photon flux and do not significantly depend on the nature of the substrate or the reaction conditions. Therefore, for a relatively constant photochemical contribution, the slower the dark reaction is, the greater the effect of photoinduced pathways results.

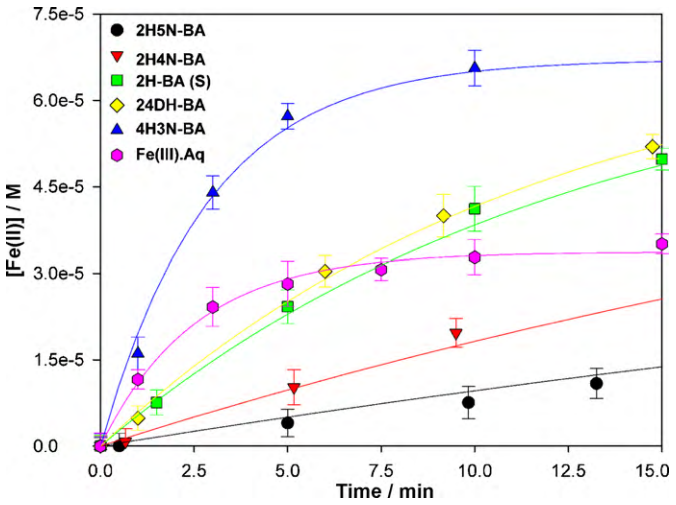

Fig. 4. Production of Fe(II) during irradiation of ferric complexes of the model substrates and of the Fe(III)–aquo complex ($Fe(III)_{aq}$) in the absence of H_2O_2. Reaction conditions: $[S]_0 = 0.1$ mM, $[Fe(III)]_0 = 0.1$ mM, pH 3.0, $T = 24\,^{\circ}C$, HPK 125 lamp with Pyrex sleeve.

3.3. Photoinduced formation of ferrous ions

To further understand the role of Fe(III) photoreduction in photo-Fenton systems and with the aim of assessing the effect of Fe(III)-complex formation on Fe(II) production, an additional set of experimental runs were planned. Concentration profiles of Fe(II) were studied in the absence of H_2O_2, since ferrous species react very quickly through Reaction (R1) in the presence of this additive [42]. In contrast, in H_2O_2-free solutions [43,44] the oxidation of Fe(II) by dissolved oxygen or by species formed in the reaction mixture is comparatively much slower.

3.3.1. Fe(II) formation in H_2O_2-free systems

Fig. 4 compares Fe(II) concentration profiles obtained by the irradiation of H_2O_2-free solutions of Fe(III) and the different substrates. For comparison purposes, a control experiment was carried out with the ferric–aquo complex in the absence of model substrate. During the first 6 min the amounts of produced Fe(II) decreased in the following order:

$$4H3N\text{-}BA > Fe(III)_{aq} > 24DH\text{-}BA \approx 2H\text{-}BA > 2H4N\text{-}BA > 2H5N\text{-}BA$$

where $Fe(III)_{aq}$ stands for the predominant ferric–aquo complex at pH 3 ($[Fe(H_2O)_5(HO)]^{2+}$). It should be emphasized that, although different sets of comparative tests were conducted using initial substrate and Fe(III) concentrations ranging from 10^{-4} to 10^{-3} M, the reactivity order at early irradiation stages was independent of the initial concentrations used. Thus, despite both the amounts of absorbed radiation and the concentration-dependent stoichiometry of some Fe(III) complexes, the reactivity order was not altered. These results suggest that inner-filter effects and differences in the complexation stoichiometries do not play a decisive role in the observed trends.

Fig. 4 shows that for timescales larger than 10 min, three substrates (4H3N-BA, 24DH-BA and 2H-BA) produced larger amounts of Fe(II) than $Fe(III)_{aq}$. On the other hand, the other substrates (2H4N-BA and 2H5N-BA) produced a much smaller amount of Fe(II). This behavior reveals that the presence of substrates of different chemical structure remarkably affects the iron cycle in these systems. The particular case of 4H3N-BA is noteworthy: this compound does not form Fe(III) complexes and thus only acts as an internal filter of radiation for $Fe(III)_{aq}$. Therefore, the higher Fe(II) amount observed in the presence of this substrate with respect to the substrate-free Fe(III) solution cannot be related to photochemical processes. It is important to recall that these trends have been observed for all the experimental conditions tested that involve a wide range of concentrations.

Finally, HPLC analyses of the solutions used in the experiments presented in Fig. 4 show that the substrates were consumed during the irradiation (substrate conversion degrees ranging from 2.4 to 5.3% at 6 min). As mentioned above, Fe(III)–aquo complexes produce HO• radicals as Fe(III) is photoreduced [6,20,38,39] (Reaction (R9)) and this could also be the case for the complexes of Fe(III) with our model substrates as they possess water ligands. Hence, the oxidation of the substrates by the HO• formed (Reaction (R3)) may produce intermediate species capable of reducing Fe(III). For this reason, except for $Fe(III)_{aq}$ solutions, the observed trends of Fe(II) production do not only correspond to photochemical processes but, in line with the autocatalytic decays obtained in Fenton systems, are highly correlated with the *in situ* generation of reducing intermediates capable of modifying the proportion of Fe(II) and Fe(III) in the reaction mixture [44].

3.3.2. Fe(II) formation in the presence of an HO• scavenger

With the aim of decreasing the effect of reducing intermediates on Fe(II) production, irradiation experiments were conducted in the presence of an HO• scavenger. Benzene was selected for this purpose due to its relatively low absorption at $\lambda > 300$ nm and because it does not form Fe(III) complexes. By using benzene concentrations up to 19 mM (near its solubility limit), HO• were effectively scavenged since HPLC analyses showed that the degradation of the substrates was negligible, the conversion degrees being in all cases lower than 2.5% after 35 min of irradiation. Therefore, the contribution of reducing intermediates derived from the model substrates to the production of Fe(II) can be neglected.

Fig. 5 shows the concentration profiles of Fe(II) obtained during the first 15 min of irradiation. In the presence of the scavenger, Fe(II) concentrations follow the trend:

$$Fe(III)_{aq} > 4H3N\text{-}BA > 2H\text{-}BA \approx 24DH\text{-}BA > 2H4N\text{-}BA > 2H5N\text{-}BA$$

Interestingly, in this case, the reactivity order was also independent of the substrate concentrations used (between 2×10^{-4} and 10^{-3} M). Additionally, in agreement with the HPLC analysis, the initial and final UV/vis absorption spectra of the substrate solutions irradiated in the presence of the scavenger do not show significant

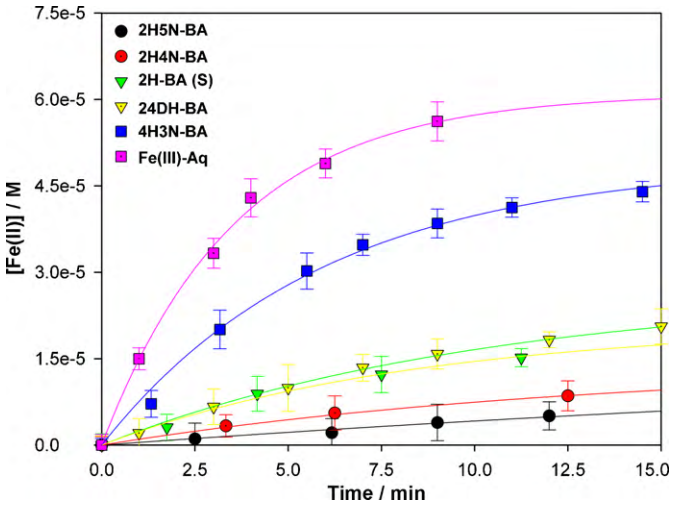

Fig. 5. Production of Fe(II) during irradiation of ferric complexes of the model substrates and of the Fe(III)–aquo complex ($Fe(III)_{aq}$), in the absence of H_2O_2 and in the presence of benzene (19 mM) as an hydroxyl radical scavenger. Reaction conditions: $[S]_0 = 0.2$ mM, $[Fe(III)]_0 = 0.1$ mM, pH 3.0, $T = 24\,^{\circ}C$, HPK 125 lamp with Pyrex sleeve.

changes at $\lambda > 300$ nm in the measured timescales. Therefore, the photonic flux available for Fe(III) photoinduced reduction remains practically constant and equal to its initial value during these experiments. The fact that the reactivity order does not depend on the acid concentrations used but on the presence or the absence of an HO• scavenger confirms that the formation of Fe(III)-reducing intermediates is critical for the observed Fe(II) production trends.

It should be pointed out that, according to the efficiencies of Fe(II) photoproduction we would have expected a much higher stability for 2H4N-BA than for 2H-BA and 24DH-BA in photo-Fenton systems (Fig. 3). Nevertheless, the relatively low stability of 2H4N-BA is associated with the contribution of dark reactions since this substrate quickly enters the fast phase even in the absence of irradiation (Fig. 2) because of the formation of Fe(III)-reducing intermediates during the early stages of its degradation.

The amount of Fe(II) produced was, as expected, lower in the presence of the HO• scavenger (Fig. 4 versus Fig. 5), except for $Fe(III)_{aq}$. In particular, the amount of Fe(II) produced was quite low for the nitrated substrates that form complexes with Fe(III).

It should be noted that there is a higher Fe(II) production from $Fe(III)_{aq}$ solutions saturated with benzene than in benzene-free solutions. In the former case, HPLC measurements show the formation of secondary products such as dihydroxybenzenes. Thus, the formation of reducing intermediates derived from the scavenger may be the cause of the higher Fe(II) production observed for benzene-saturated $Fe(III)_{aq}$ solutions. Therefore, the addition of benzene did not result in a complete suppression of the dark Fe(III)-reducing reactions (i.e., (R7)).

3.4. Role of reaction intermediates and photoreduction efficiencies

As indicated above, the profiles of Fig. 4 suggest an important contribution of dark reactions to Fe(III) reduction. Such contribution is associated with intermediate products generated by oxidation of the particular model substrates as the irradiation proceeds, the only exception being $Fe(III)_{aq}$, which after 6 min showed a plateau for [Fe(II)] since reducing intermediates cannot be formed. Hence, both the aforementioned relatively low "inner-filter effects" and the noticeable increases of Fe(II) production in the absence of an HO• scavenger lead to the conclusion that the degradation intermediates of the model substrates (RI_S) enhance the production of Fe(II) through dark reactions such as:

$$S + HO^{\bullet} \rightarrow RI_S \quad \text{(R13)}$$

$$RI_S + Fe(III) \rightarrow Fe(II) + P_S \quad \text{(R14)}$$

where RI_S and P_S stand for Fe(III)-reducing intermediates formed from the model substrates and their oxidized products, respectively.

In contrast, for the experiments shown in Fig. 5, which were conducted in the presence of benzene, Fe(III)-reducing intermediates are formed from the HO• scavenger:

$$BEN + 2HO^{\bullet} \rightarrow\rightarrow HQ/CAT \quad \text{(R15)}$$

$$HQ/CAT + 2Fe(III) \rightarrow 2Fe(II) + p/o\text{-}BQ \quad \text{(R16)}$$

where BEN, HQ, CAT and BQ stand for benzene, hydroquinone, catechol and benzoquinone, respectively.

Given the high scavenger concentration used (Fig. 5), the contribution of degradation intermediates of each particular substrate to Fe(II) production may be neglected. In addition, the Fe(III)-reducing intermediates formed in the presence of benzene (R15) are the same, independently of the model substrate tested. However, their production is strongly dependent on the photoactivity of the irradiated iron complex. Therefore, the profiles shown in Fig. 5 are undoubtedly much more representative of Fe(III) photoreduction efficiencies than the profiles shown in Fig. 4.

The experiments of Fig. 5 suggest that the photoreduction of the Fe(III) complexes formed with the model substrates is less efficient than the photoreduction of $Fe(III)_{aq}$. The latter trend is in line with the results obtained by other authors in photo-electro-Fenton treatments [45]. Finally, the results show that the photoreduction efficiencies of the complexes formed with the nitro derivatives (2H4N-BA and 2H5N-BA) are lower than those corresponding to the nonnitrated ones (2H-BA and 24DH-BA).

The photoenhancement sequence 4H3N-BA > 24DH-BA > 2H4N-BA (Table 3) agrees with the order of Fe(II) photoproduction (Figs. 4 and 5) since in dark Fenton-like systems these compounds exhibit, for conversion degrees between 20 and 70%, very similar decay profiles (Fig. 2). In contrast, when nonphotochemical processes have dissimilar contributions, no relationship necessarily exists between Fe(II) photoproduction efficiency and the photoenhancement factor. Indeed, although photoreduction efficiencies of Fe(III) complexes with 2H-BA and 24DH-BA are practically identical, the photoenhancement factor is greater for 2H-BA than for 24DH-BA, since 2H-BA displays a much longer slow phase in Fenton-like systems. Finally, the inversion observed for Fe(II) production between $Fe(III)_{aq}$ and 4H3N-BA in Figs. 4 and 5 can be explained by taking into account both the inner-filter effects (which are evident from Fig. 5 and are in line with the absorption of 4H3N-BA at $\lambda > 300$ nm) and the strong contribution of the intermediates of 4H3N-BA oxidation to the profiles shown in Fig. 4. This is in agreement with the fact that, although 4H3N-BA has the lowest reactivity towards HO• radicals, it exhibits the shortest slow phase among the studied substrates in both Fenton-like and photo-Fenton systems (Figs. 2 and 3).

4. Conclusions

In this work, we carried out a comparative investigation of the degradation kinetics of hydroxy and hydroxynitro derivatives of benzoic acid in Fenton-like and photo-Fenton systems. Autocatalytic profiles were observed for the substrates and H_2O_2 consumption in both processes, the contribution of dark reactions (i.e., nonphotochemical processes) being decisive even in photo-Fenton systems. A simple equation that may be used as a valuable tool for a semiquantitative analysis of the main kinetic features of inverted "S" decays, as well as a method for the estimation of the relative contribution of photoinduced pathways in photo-Fenton systems (photoenhancement factors), are proposed. Hence, Eqs. (8) and (12) may be useful for a comprehensive design of efficient wastewater purification methodologies.

Although both speciation and reactivity towards HO• may be important factors affecting the kinetic behavior, from the complementary studies performed to evaluate acid–base properties, ferric complex formation, reactivity towards HO• and Fe(II) photoproduction efficiencies, it can be stated that the overall oxidation rates of the substrates investigated in photo-Fenton systems are not correlated with the reactivities towards HO• radicals. These rates are mainly governed by the formation of degradation intermediates capable of reducing Fe(III), and, to a lesser extent, by the contribution of photoinduced processes whose relative importance depends on both the photoreduction efficiencies of Fe(III) complexes and the inner-filter effects.

Acknowledgements

This research was partially supported by the France-Argentina exchange program ECOS-MINCyT (Project ECOS No. A07E07) and Argentinean ANPCyT (Project No. PICT 33919). D. Nichela thanks

the CONICET for her research graduate grant. F.S. García Einschlag is research member of CONICET and E. Oliveros of CNRS.

Appendix A. Supplementary data

Supplementary data associated with this article can be found, in the online version, at doi:10.1016/j.apcatb.2010.05.026.

References

[1] C. von Sonntag, Water Sci. Technol. 58 (2008) 1015–1021.
[2] O. Legrini, E. Oliveros, A.M. Braun, Chem. Rev. 93 (1993) 671–698.
[3] C. Walling, Acc. Chem. Res. 8 (1975) 125–131.
[4] D. Nichela, L. Carlos, F.S. García Einschlag, Appl. Catal. B 82 (2008) 11–18.
[5] L. Carlos, D. Fabbri, A.L. Capparelli, A.B. Prevot, E. Pramauro, F.S. García Einschlag, Chemosphere 72 (2008) 952–958.
[6] J.J. Pignatello, E. Oliveros, A. MacKay, Crit. Rev. Environ. Sci. Technol. 36 (2006) 1–84.
[7] E. Neyens, J. Baeyens, J. Hazard. Mater. 98 (2003) 33–50.
[8] A. Georgi, A. Schierz, U. Trommler, C.P. Horwitz, T.J. Collins, F.D. Kopinke, Appl. Catal. B 72 (2007) 26–36.
[9] H. Gallard, J. De Laat, B. Legube, Water Res. 33 (1998) 2929–2936.
[10] H. Gallard, J. De Laat, Chemosphere 42 (2001) 405–413.
[11] F.J. Rivas, F.J. Beltran, J. Frades, P. Buxeda, Water Res. 35 (2001) 387–396.
[12] N. Kang, D.S. Lee, J. Yoon, Chemosphere 47 (2002) 915–924.
[13] Y.X. Du, M.H. Zhou, L.C. Lei, J. Hazard. Mater. 136 (2006) 859–865.
[14] F. Chen, W.H. Ma, J.J. He, J.C. Zhao, J. Phys. Chem. A 106 (2002) 9485–9490.
[15] J.H. Ma, W.J. Song, C.C. Chen, W.H. Ma, J.C. Zhao, Y.L. Tang, Environ. Sci. Technol. 39 (2005) 5810–5815.
[16] K.Q. Wu, Y.D. Xie, J.C. Zhao, H. Hidaka, J. Mol. Catal. A: Chem. 144 (1999) 77–84.
[17] H. Liu, X.Z. Li, Y.J. Leng, C. Wang, Water Res. 41 (2007) 1161–1167.
[18] A. Goi, Y. Veressinina, M. Trapido, Chem. Eng. J. 143 (2008) 1–9.
[19] A. Serra, X. Domènech, C. Arias, E. Brillas, J. Peral, Appl. Catal. B 89 (2009) 12–21.
[20] V. Kavitha, K. Palanivelu, J. Photochem. Photobiol. A 170 (2005) 83–95.
[21] J.J. Pignatello, Environ. Sci. Technol. 26 (1992) 944–951.
[22] J. Sima, J. Makanova, Coord. Chem. Rev. 160 (1997) 161–189.
[23] Y. Kamaya, Y. Fukaya, K. Suzuki, Chemosphere 59 (2005) 255–261.
[24] F. BenoitMarquie, E. PuechCostes, A.M. Braun, E. Oliveros, M.T. Maurette, J. Photochem. Photobiol. A 108 (1997) 65–71.
[25] A. Di Paola, V. Augugliaro, L. Palmisano, G. Pantaleo, E. Savinov, J. Photochem. Photobiol. A 155 (2003) 207–214.
[26] C.C. Allain, L.S. Poon, C.S.G. Chan, W. Richmond, P.C. Fu, Clin. Chem. 20 (1974) 470–475.
[27] M. Rios-Enriquez, N. Shahin, C. Durán-de-Bazúa, J. Lang, E. Oliveros, S.H. Bossmann, A.M. Braun, Solar Energy 77 (2004) 491–501.
[28] J.J. Pignatello, D. Liu, P. Huston, Environ. Sci. Technol. 33 (1999) 1832–1839.
[29] F.S. García Einschlag, L. Carlos, A.L. Capparelli, Chemosphere 53 (2003) 1–7.
[30] V.M. Nurchi, T. Pivetta, J.I. Lachowicz, G. Crisponi, J. Inorg. Biochem. 103 (2009) 227–236.
[31] R. Aydin, U. Özer, N. Türkel, Turk. J. Chem. 21 (1997) 428–436.
[32] K.S. Lee, D.W. Lee, Anal. Chem. 46 (1974) 1903–1908.
[33] N. Hirayama, T. Kuwamoto, Anal. Chem. 65 (1993) 141–147.
[34] M.A. Oturan, J. Pinson, J. Phys. Chem. 99 (1995) 13948–13954.
[35] R.Z. Chen, J.J. Pignatello, Environ. Sci. Technol. 31 (1997) 2399–2406.
[36] D. Prato-Garcia, R. Vasquez-Medrano, M. Hernandez-Esparza, Solar Energy 83 (2009) 306–315.
[37] L. Carlos, D. Fabbri, A.L. Capparelli, A.B. Prevot, E. Pramauro, F.G. Einschlag, J. Photochem. Photobiol. A-Chem. 201 (2009) 32–38.
[38] H.J. Benkelberg, P. Warneck, J. Phys. Chem. 99 (1995) 5214–5221.
[39] L. Lopes, J. de Laat, B. Legube, Inorg. Chem. 41 (2002) 2505–2517.
[40] L. Wang, C. Zhang, H. Mestankova, F. Wu, N. Deng, M.B. Gang Pan, G. Mailhot, Photochem. Photobiol. Sci. 8 (2009) 1059–1065.
[41] M. Skoumal, C. Arias, P.L. Cabot, F. Centellas, J.A. Garrido, R.M. Rodríguez, E. Brillas, Chemosphere 71 (2008) 1718–1729.
[42] A. Machulek, J.E.F. Moraes, L.T. Okano, C.A. Silverio, F.H. Quina, Photochem. Photobiol. Sci. 8 (2009) 985–991.
[43] R. Andreozzi, R. Marotta, Water Res. 38 (2004) 1225–1236.
[44] G. Mailhot, L. Hykrdova, J. Jirkovsky, K. Lemr, G. Grabner, M.B. Bolte, Appl. Catal. B 50 (2004) 25–35.
[45] E. Guinea, C. Arias, P.L. Cabot, J.A. Garrido, R.M. Rodriguez, F. Centellas, E. Brillas, Water Res. 42 (2008) 499–511.